

# The metabolome alters the thermodynamic and chemical stability of RNA

complex

**ABSTRACT:** Herein, we examine the complicated network of interactions among RNA, the metabolome, and the metalome in conditions that mimic the *E. coli* cytoplasm. First, we determined Mg<sup>2+</sup> binding constants for the top 15 *E. coli* metabolites, comprising 80% of the total metabolome, at physiological pH and monovalent ion concentrations. Then, we used this information to inform creation of artificial cytoplasms that mimic *in vivo* *E. coli* conditions, termed Eco80. We empirically determined that the mixture of *E. coli* metabolites in Eco80 approximates single site binding behavior towards Mg<sup>2+</sup> in the biologically relevant free Mg<sup>2+</sup> range of ~0.5 to 3 mM Mg<sup>2+</sup>, using a Mg<sup>2+</sup> binding fluorescent dye (8-Hydroxy-5-quinolinesulfonic acid). Furthermore, we examined the effects of Eco80 conditions on the thermodynamic stability, chemical stability, catalysis, and compactness of RNA. We find that these Eco80 conditions lead to opposing effects, where the thermodynamic stability of RNA helices were weakened but chemical stability, compactness, and catalysis were enhanced. We propose a mechanism where increased RNA compactness and catalysis is facilitated in Eco80.

## Introduction

on the thermodynamic and chemical stabilities of RNA.

Too much detail for the Abstract  
were measured

Summary of progress on *in vivo*-like conditions. (ref Kate's QR&B review.)

Studies that consider cellular components one at a time.

Studies that consider cellular components together in artificial cytoplasm.

These behaviors enhance RNA function and conformational changes.

In contrast, we take a bottom up, *aufbau*, approach that builds up complexity, to make an artificial cytoplasm that contains 80% of *E. coli* metabolites with biologically relevant concentrations of monovalent ions and free Mg<sup>2+</sup> ions. This *aufbau* approach allows us to understand the effects of 80% of metabolite and metal ion species that compose a part of the network of interactions that RNA experiences in *E. coli* cells.

**Eco80: An artificial cytoplasm containing 80% of *E. coli* metabolites** discuss other bottom up but these have been simplified because of need to accommodate 260nm Results (?) E. coli cells contain hundreds of metabolites (about 240 mM total), which is too many metabolites to test systematically. However, 15 abundant metabolites, an experimentally manageable number, comprise 80% (195 mM) of total metabolites (Figure 1A). Thus, we sought to prepare Eco80, an artificial cytoplasm containing the biological concentrations of the 15 most abundant metabolites in *E. coli* (Table 1).

All of the metabolites in Eco80 are zwitterions, or negatively charged, near physiological pH (~7) and require electrostatic neutralization with metal ions. We prepared Eco80 so that the final monovalent ion concentration was the physiological value of 240 mM Na<sup>+</sup> and 140 mM K<sup>+</sup> (Supplementary information (SI) Table 1). Metabolite salts and free acids were prepared to a final 2x concentration, and the amount of Na<sup>+</sup> and K<sup>+</sup> added with each metabolite was recorded. Next, the pH of the 2x stock was adjusted to pH 7.0 using NaOH, and the amount of Na<sup>+</sup> was recorded. Lastly, NaCl and KCl were added to a final 240 mM Na<sup>+</sup> and 140 mM K<sup>+</sup>. We thus created Eco80, at a 2x final concentration so that it could be diluted into other reagents for experiments.

Next, we considered how metabolites affect the speciation of free and chelated Mg<sup>2+</sup>. All 15 Eco80 metabolites have functional groups, carboxylates and phosphates, that drive chelating interactions with Mg<sup>2+</sup> ions (Table 1), and we have previously estimated that the metabolite pool in *E. coli* has potential to chelate 51 mM Mg<sup>2+</sup>, assuming 2 mM free Mg<sup>2+</sup>, at an ionic strength of 0.15 M and a pH of 7.5. While extensive literature exists on chelating interactions between Mg<sup>2+</sup> and small molecules, our previous estimates are putative as Mg<sup>2+</sup> binding affinity is dependent on environmental factors such as pH, ionic strength, the composition of background ions, and temperature. Thus, we sought to better characterize Mg<sup>2+</sup> chelation by the metabolites in Eco80, at the physiological background.

We determined apparent dissociation constants ( $K_D$ ) for Eco80 metabolites in 240 mM NaCl, 140 mM KCl, pH 7.0 buffer at 37 °C (Table 1). Isothermal titration calorimetry (ITC) was used to determine  $K_D$ s for phosphorylated metabolites (SI figure 1, SI Table 2). A fluorescence assay, that measures the free Mg<sup>2+</sup> concentration in a sample using the metal ion binding dye 8-Hydroxy-5-quinolinesulfonic (HQS) acid, was used to estimate the  $K_D$  for Mg<sup>2+</sup> of metabolites that did not produce enough heat on binding Mg<sup>2+</sup> to measure

+ of your technique! 260nm

= II

see Methods

for details.

Briefly,

with ITC (SI figure 2, SI Table 3). For the HQS assay,  $Mg^{2+}$  is titrated into HQS solutions in the absence and presence of chelators. HQS emission as a function of the total  $Mg^{2+}$  in the absence of chelators is then fit to a binding model (SI figure 2A, top blue data and black fit). The free  $Mg^{2+}$  concentration is then calculated from the fluorescence emission for each data point using the binding model, providing the free  $Mg^{2+}$  concentration as a function of the total  $Mg^{2+}$  concentration (SI figure 2A, bottom).  $Mg^{2+}$  binding by metabolites is thus observed by fitting the free  $Mg^{2+}$  concentration as a function of the total  $Mg^{2+}$  concentration, which is shifted to the right as  $Mg^{2+}$  is sequestered by metabolites.

The four nucleotide triphosphates, ATP, UTP, GTP, and dTTP, were classified as strong  $Mg^{2+}$  binders, with  $K_D$  values less than the approximate free  $Mg^{2+}$  concentration in *E. coli* (2 mM) (Table 1). Conversely, 8 other metabolites, L-glutamic acid, fructose 1,6-BP, UDP-N-acetylglucosamine, Glucose 6-phosphate, L-aspartic acid, 6-Phospho-gluconic acid, dihydroxyacetone phosphate, and pyruvic acid, were classified as weak  $Mg^{2+}$  binders, with a  $K_D$  value greater than 2 mM (Table 1). Three metabolites, glutathione, L-valine, and L-glutamine had negligible  $Mg^{2+}$  binding properties, as measured with HQS (SI figure 2). We thus broke Eco80 down into two other artificial cytoplasm: NTP-chelated  $Mg^{2+}$  (NTPCM), and weak-metabolite chelated  $Mg^{2+}$  (WMCM), composed of the strong  $Mg^{2+}$  chelators (NTPs), and weak  $Mg^{2+}$  chelators, respectively (Table 1).

In an effort to understand effects of Eco 80 on RNA stability

We next used two methods to estimate how Eco80 metabolites affect the speciation of free and chelated  $Mg^{2+}$  as a mixture. The first method was experimental, using HQS emission to estimate the free  $Mg^{2+}$  concentration in the presence of metabolites (Figure 1B-C, SI Table 3). The second method was a statistical model that accounts for experimental uncertainty in metabolite concentrations and uncertainty in  $K_D$  determination, based on single-site binding (meaning that one metabolite associates one  $Mg^{2+}$ ). The statistical model is described in detail in the Supplementary Methods. Briefly, concentration errors were propagated from uncertainties in reagent masses and volumes used during sample preparation, and  $K_D$  uncertainties were obtained from the fits (Table 1). Both uncertainties were then randomly seeded into Equation 1 to create 1000 virtual artificial cytoplasms, where  $[Mg]_T$  is the total  $Mg^{2+}$  concentration,  $[Mg]$  is the free  $Mg^{2+}$  concentration,  $i$  is an integer representing each metabolite in a mixture,  $N$  is the total number of metabolites in a mixture,  $[L_i]_T$  is the concentration of the "i'th" metabolite in a mixture, and  $K_D$  is the disassociation constant.

$$[Mg]_T = [Mg] + \sum_{i=1}^N \frac{[L_i]_T [Mg]}{K_{D,i} + [Mg]} \quad [1]?$$

Then, equation 1 is solved numerically to determine the free  $Mg^{2+}$  concentration produced at a given total  $Mg^{2+}$  concentration in a virtual artificial cytoplasm.

Add Science & Nature ref (Langford et al 2018) free concentration

Indeed, the metabolites buffer the  $Mg^{2+}$  in which

a 40% increase in  $Mg^{2+}$  results in only a 2.5% increase in free  $Mg^{2+}$ . This is true in Eq 1? (True?)

The two methods indicate that  $Mg^{2+}$  speciates in artificial cytoplasms according to a single-site model within or below the biological free  $Mg^{2+}$  range of 0.5 to 3 mM  $Mg^{2+}$ , but not at higher free  $Mg^{2+}$  concentrations (Figure 1 E-F). For example, in Eco80, the statistical model suggests that the free  $Mg^{2+}$  should increase slowly as the total  $Mg^{2+}$  concentration is increased, until the strong  $Mg^{2+}$  chelators (NTPs) become saturated at about 27 mM total  $Mg^{2+}$  (Figure 1E, hex bins). At total  $Mg^{2+}$  concentrations higher than 27 mM, the free  $Mg^{2+}$  should increase faster because the NTPs are saturated by  $Mg^{2+}$  and the weak chelators sequester less  $Mg^{2+}$ . Free  $Mg^{2+}$ , calculated using HQS emission shows a similar trend to the statistical model below 3 mM  $Mg^{2+}$  free (Figure 1E, data points). However, the free  $Mg^{2+}$  concentration calculated from HQS emission does not increase with the total  $Mg^{2+}$  as fast as the single-site model would predict above 3 mM free  $Mg^{2+}$ , indicating the action of such multivalent interactions, where one metabolite interacts with several  $Mg^{2+}$  molecules, dominate the equilibrium. Non-single-site behavior above 3 mM free  $Mg^{2+}$  is also observed in the NTPCM and WMCM artificial cytoplasms (Figure 1 F & G), and was observed previously in

Ryota Nat. Comm.

Lastly, we sought to empirically determine how much total  $Mg^{2+}$  is required to maintain a free  $Mg^{2+}$  concentration of 2 mM in Eco80, NTPCM, and WMCM. The relationship between the free  $Mg^{2+}$  calculated from HQS emission and the total  $Mg^{2+}$  concentration was fit to a polynomial to empirically approximate the data (Figure 1 E-G, colored lines), and the total  $Mg^{2+}$  concentration required to produce 2 mM Free  $Mg^{2+}$  was calculated from the polynomial fit. This resulted in predicted 31.6, 25.0, and 6.5 mM total  $Mg^{2+}$  concentration to produce 2 mM free  $Mg^{2+}$  in Eco80, NTPCM, and WMCM, respectively (Table 2).

### Thermodynamic analysis of RNA helices in Eco80

We sought to understand how Eco80 affects the stability of RNA helices composed of Watson-Crick base pairs. RNA helix stability is traditionally measured with UV-absorbance melting curves, usually at 260 or 280 nm, which allows for accurate calculation of helix folding energies. However, absorbance melting curves were not appropriate for measuring helix stability in Eco80 because of the high absorbability of ATP, UTP, GTP, dTTP, and UDP-N-acetylglucosamine. Thus we used a fluorescence binding isotherm assay, which is optically orthogonal to Eco80.

Helix stability was measured using the emission of a 5'-fluorophore labeled RNA strand (FAM-RNA) in equilibrium with a complementary 3'-quencher labeled RNA strand (RNA-BHQ1), (Figure 2A). High emission indicates that the FAM-RNA is single-stranded while low emission indicates that the FAM-RNA is bound in duplex with a RNA-BHQ1 strand (Figure 2A). We used a binding isotherm method, where RNA-BHQ1 is titrated into a constant concentration of FAM-RNA at a single temperature (SI figure 3), resulting in an apparent binding isotherm (Figure 2B). Fluorescence binding isotherms were favored over fluorescence melts because of the unpredictable dependence of FAM emission on temperature. FAM emission was monitored in a Real-Time PCR instrument at different temperatures, resulting in a isotherm every 0.5 °C from 20 to 80 °C (Figure 2B). Fluorescence isotherms were fit at each temperature to SI equation X, thus determining the  $K_D$  between the FAM-RNA strand and the RNA-BHQ1 strand.

Raw fluorescence was fit with a new program called MeltR, created by the authors, to determine folding energies. MeltR is a package of functions in the popular R programming language, that allows facile conversion of raw data to folding energies. Importantly, MeltR handles two sources of experimental error, uncertainty in RNA concentration and inaccurate  $K_D$ s collected at low and high temperatures. MeltR then calculates folding energies using two Van't Hoff methods, directly fitting a Van't Hoff plot (Figure 3C) and globally fitting raw fluorescence emission to SI equation X.

We found that helix energies from fitting fluorescence binding isotherms are highly dependent on the errors in the determination of RNA concentrations in stock solutions, which is propagated systematically during sample preparation (SI Figure 3). To understand why, we modeled data assuming a folding enthalpy ( $\Delta H$ ), entropy ( $\Delta S$ ), and Gibb's free energy at 37 °C ( $\Delta G^{37\text{°C}}$ ) of -56.2 kcal/mol, -136.4 cal/mol/K, and -13.9 kcal/mol respectively, 5% random fluorescence error, and perfectly accurate determination of RNA concentrations in concentrated stocks (a 200 nM FAM-RNA concentration, and 0, 1, 10, 50, 100, 150, 200, 250, 400, 600, 800, and 1000 nM RNA-BHQ1 concentrations). We then used MeltR to fit the modeled data, resulting in accurate determination of  $\Delta H = -56.0$  kcal/mol,  $\Delta S = -135.7$  cal/mol/K, and  $\Delta G = -13.9$  kcal/mol. We next considered how assuming incorrect RNA stock concentrations, thus incorporating a systematic error, could effect the accuracy of the fits. Systematic error (-50% to +50%) was seeded into virtual stock concentrations and the data were refit (SI figure 4A). We found that fit accuracy what highly dependent on error in stock concentrations, unless the FAM-RNA error and the RNA-BHQ1 error compensated for each other, e.g. %RNA-BHQ1 error = %FAM-RNA error. (Walk us through limits)

We next considered a more realistic scenario, where the experiment assumes perfectly accurate determination of RNA concentrations but there is actually +20% FAM-RNA concentration error. Data was modeled using the same folding energies and RNA-BHQ1 concentrations, but with a 240 nM FAM-RNA

*not as bad as ΔH and ΔS errors.*

concentration (+20% error). We then used MeltR to fit the modeled data, assuming a 200 nM FAM-RNA concentration, resulting in inaccurate determination of  $\Delta H = -35.8$  kcal/mol,  $\Delta S = -75.5$  cal/mol/K, and  $\Delta G = -12.3$  kcal/mol. Once again, we seeded systematic error (-50% to +50%) into virtual stock concentrations and the data were refit (SI figure 4B). Similar to SI figure 4A, we found that fit accuracy was highly dependent on errors in stock concentrations. However, the fits were most accurate according to Equation 1 instead of where %RNA-BHQ1 error = %FAM-RNA error:

$$\%BHQ1_{error} = \frac{1}{X} \%FAM_{error} + \frac{100 - 100X}{X}$$

Where X is the actual FAM-RNA concentration divided by the estimated FAM-RNA concentration (240 nM/200 nmol = 1.2 in this example). Thus, MeltR does not need perfectly accurate concentrations, just an optimization algorithm that finds the FAM-RNA concentration correction factor X. To find X, MeltR selects an isotherm (usually the lowest temperature), where the  $K_D$  is more than 10 times less than the FAM-RNA labeled concentration (SI figure 4C). At this  $K_D$  range, the shape of the binding curve is independent of  $K_D$ , and MeltR uses the isotherm as a Job plot to determine X. MeltR then uses X to correct the FAM-RNA concentration. We next tested the MeltR optimization algorithm. The modeled data, with +20% FAM-RNA concentration error, was fit using MeltR with the concentration optimization algorithm on, resulting in an accurate determination of  $\Delta H = -51.9$  kcal/mol,  $\Delta S = -123.5$  cal/mol/K, and  $\Delta G = -13.6$  kcal/mol. We then seeded additional error into the data set (-50% to +50%), refit the data using the MeltR concentration optimization algorithm, and found that MeltR calculates accurate folding energies (within 0.2 kcal/mol in terms of the  $\Delta G$ ) even with large inaccuracies in reagent concentration estimates (SI Figure 4D).

MeltR then filters out isotherms that produce inaccurate  $K_D$ s, according to user specifications. Fits are first filtered by magnitude because fits  $K_D$ s are most accurate in the range of more than the FAM-RNA concentration/10 and less than the FAM-RNA concentration times 10 (SI figure 5).  $K_D$ s below the FAM-RNA concentration/10 are inaccurate because the shape of the isotherm curve is independent of the  $K_D$ , as the FAM-RNA stand is stoichiometrically bound by RNA-BHQ1. Likewise,  $K_D$ s above 10 times the FAM-RNA concentration are also inaccurate because not enough FAM-RNA is binding to RNA-BHQ1 to generate a curve. After filtering by magnitude, MeltR filters  $K_D$ s by the standard error in the fit, so that the most accurate  $K_D$ s are used to determine folding energies. Both the MeltR  $K_D$  range, and  $K_D$  error threshold can be adjusted by the user to refine fits. For example, with the MeltR fit of the modeled data with +20% FAM-RNA concentration error and the concentration optimization algorithm on, can be improved to more accurate helix energies,  $\Delta H = -56.4$  kcal/mol,  $\Delta S = -136.9$  cal/mol/K, and  $\Delta G = -13.9$  kcal/mol

### Eco80 destabilizes RNA helices

Paragraph 1: Summary of helix energies and error propagation for values reported in Table 1

We used fluorescence binding isotherms to determine helix folding energies in background monovalent metal ion control (240 mM NaCl 140 mM KCl), Eco80, NTPCM, and WMCM, for a data set of five representative RNA helices. All solutions contain 2 mM  $Mg^{2+}$  as per Table 2. We used both methods to determine folding energies in MeltR, where method 1 was fitting the Van't Hoff relationship between the disassociation constant and temperature and method 2 was directly globally fitting the raw fluorescence binding isotherms (SI table 4). Standard errors estimated from the fit for method 1 were 1.7%, 2%, and 0.3 % on average for the  $\Delta H$ ,  $\Delta S$ , and  $\Delta G^{37^\circ C}$ . Standard errors estimated from the fit for method 2 were larger, at 21.7%, 26.5%, and 3.4 % on average for the  $\Delta H$ ,  $\Delta S$ , and  $\Delta G^{37^\circ C}$ . However, the difference in helix folding energies between the two methods between the two methods was much smaller, at 1.2%, 1.4%, and 0.2% on average for the  $\Delta H$ ,  $\Delta S$ , and  $\Delta G^{37^\circ C}$ . Given that the two methods provide similar helix folding energies, but different standard errors, the discrepancy in standard error likely reflects differences in the number of parameters that must be estimated

How different?

Break up  
Explain how chosen

# Let's Talk

1

by the fit (two for method 1,  $\Delta H$  and  $\Delta S$ , and  $2+2*\text{number of raw isotherms}$  for method 1,  $\Delta H$ ,  $\Delta S$ , and a  $F_{\max}/F_{\min}$  for each raw isotherm), more than it reflects systematic and random errors in helix folding energy estimation. Turner and colleagues estimated an uncertainty of 12%, 13.5%, and 4% for the  $\Delta H$ ,  $\Delta S$ , and  $\Delta G^{37^\circ\text{C}}$ , respectively, conservatively reflect systematic and random errors in error determination for absorbance melting curves by comparing helix energies collected on the same sequences by different labs.<sup>Ref</sup> Given that the discrepancy between method 1 and method 2 were smaller than the Turner uncertainty for all fluorescence binding isotherms in this study, and that we are determining differences between conditions on the same sequences collected in the same lab, the 4% value in terms of the is too conservative. We determined that there was on average 0.2 kcal/mol, or 1.5%, error for MeltR fitting modeled fluorescence data using the concentration optimization algorithm (SI Figure 4). Thus, we reported the  $\Delta G^{37^\circ\text{C}}$  of helix formation from method 1 with an uncertainty of 1.5% in Table 3 and the 1.5% uncertainty was propagated to the association constant in Figure 2D.

Previous section?

\* Can we add 1M NaCl expt + pred?

Talk through these data.

All five representative helices were significantly destabilized in Eco80, meaning the the  $\Delta\Delta G^{37^\circ\text{C}}$  between the background monovalent condition and Eco80 was larger than the propagated uncertainty in  $\Delta\Delta G^{37^\circ\text{C}}$ , by 0.44 to 1.12 kcal/mol (Table 3, Figure 2D). To better understand how components of Eco80 destabilize RNA helices, we then analyzed the effects of strong Mg<sup>2+</sup> chelating metabolites and weak Mg<sup>2+</sup> chelating metabolites, separately. NTPCM, which is composed of strong Mg<sup>2+</sup> chelating metabolites, consistently destabilized RNA helices (Figure 2D). Helices 1, 2, 3, and 5 were significantly destabilized by 0.41 to 0.60 kcal/mol (Table 3). NTPCM did not significantly destabilize Helix 4, however, the the 0.32 kcal/mol destabilization effect is consistent with the other 5 helices. In contrast to NTPCM, WMCM, which is composed of strong Mg<sup>2+</sup> chelating metabolites, destabilized, had no effect, or stabilized RNA helices depending on the helix identity (Figure 2D). WMCM significantly destabilized helix 3 and 4 by 0.82 and 0.40 kcal/mol respectively. No significant change in stability was observed for helices 2 and 5 in WMCM. Lastly, helix 1 was significantly stabilized in WMCM by about -0.4 kcal/mol. Thus, the net effect of Eco80 on RNA helices is destabilization, with destabilizing interactions dominating for strong Mg<sup>2+</sup> chelating metabolites, and a mixture of stabilizing and destabilizing interactions for weak Mg<sup>2+</sup> chelating metabolites.

## Eco80 protects RNA from degradation

## E. coli metabolites promote RNA compactness and RNA catalysis

### Discussion

Making Eco80 artificial cytoplasm

-Complex but manageable

Effects on helices

-Mg stabilizes (from lit)

-Polar osmolytes destabilize (from lit)

-Here we analyze their effects together and see opposing effects

Propose model that summarizes effects



Next time, group All Main text Figs and "SI" "separated"

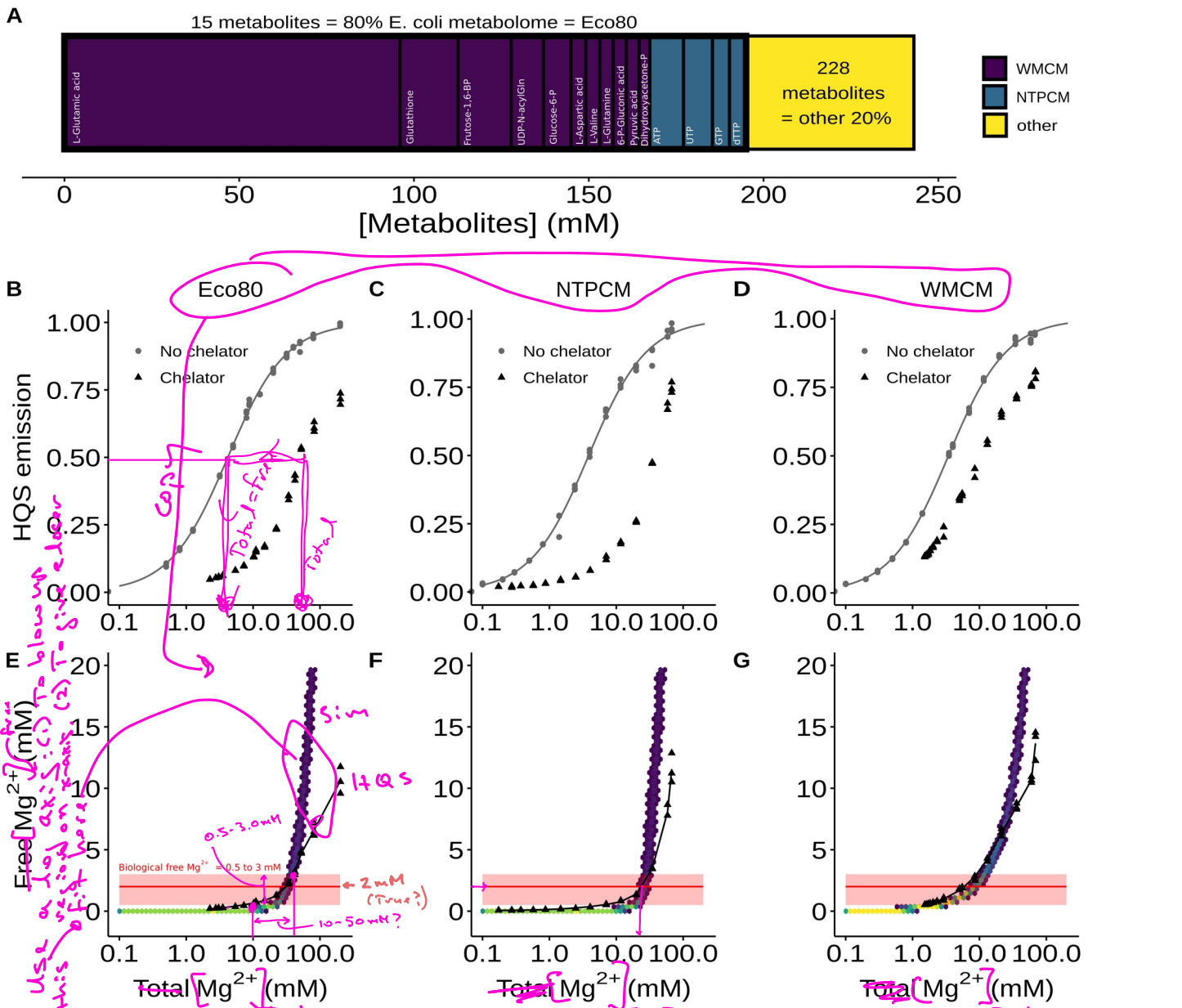


**Figure 1** Analysis of  $Mg^{2+}$  speciation in *E. coli* metabolite mixtures. Eco80 contains (A) *E. coli* metabolome molar composition. Eco80 contains the 15 most abundant metabolites that comprise 80% of the *E. coli* metabolome. NTPCM contains four strong  $Mg^{2+}$  chelating NTPs, and WMCM contains 11 other weak  $Mg^{2+}$  binding metabolites. (B-D) Effect of  $Mg^{2+}$  on 8-hydroxyquinoline-5-sulphonic acid (HQS) emission with and without mixtures of metabolites that chelate  $Mg^{2+}$ . Grey lines represent fits to determine the binding constant for  $Mg^{2+}$  and HQS in the absence of chelators. (E-G) Relationship between the total  $Mg^{2+}$  concentration and the free  $Mg^{2+}$  concentration with mixtures of metabolites that chelate  $Mg^{2+}$ . The free  $Mg^{2+}$  concentration (x-axis) was calculated using HQS emission and the binding constant for  $Mg^{2+}$  and HQS. Hex bins represent a statistical simulation of 1000 virtual artificial cytoplasmas based on experimental errors in  $K_D$  determination, experimental errors in reagent concentrations, and single site binding. Triangle data points are free  $Mg^{2+}$  concentrations calculated using HQS emission. Black lines were generated using polynomial regression. The red shaded region is the biological free  $Mg^{2+}$  concentration, 0.5 to 3 mM. The red line is the approximate free  $Mg^{2+}$  concentration in *E. coli*.

of 2 μM  
(True?)

**Table 1.** Eco80: the 15 most abundant metabolites which comprise 80% of the *E. coli* metabolome.

Metabolite	Conc. (mM)	$K_D$ (mM)	Chelation strength
ATP	9.63 (0.963) <sup>a</sup>	0.28 (0.01) <sup>b</sup>	NTPCM (Strong) <sup>c</sup>
UTP	8.29 (0.829) <sup>b</sup>	0.248 (0.004) <sup>b</sup>	NTPCM (Strong) <sup>b</sup>
GTP	4.87 (0.487) <sup>b</sup>	0.201 (0.007) <sup>b</sup>	NTPCM (Strong) <sup>b</sup>
dTTP	4.62 (0.462) <sup>b</sup>	0.160 (0.003) <sup>b</sup>	NTPCM (Strong) <sup>b</sup>
L-Glutamic acid	96 (9.6) <sup>b</sup>	520 (50) <sup>c</sup>	WMCM (Weak) <sup>b</sup>
Glutathione	16.6 (1.66) <sup>b</sup>	NA <sup>d</sup>	WMCM (Weak) <sup>b</sup>
Fructose 1,6- bisphosphate	15.2 (1.52) <sup>b</sup>	5.9 (0.1) <sup>b</sup>	WMCM (Weak) <sup>b</sup>
UDP-N- acetylglucosamine	9.24 (0.924) <sup>b</sup>	29 (2) <sup>b</sup>	WMCM (Weak) <sup>b</sup>
Glucose 6-phosphate	7.88 (0.788) <sup>b</sup>	17.3 (0.2) <sup>b</sup>	WMCM (Weak) <sup>b</sup>
L-Aspartic acid	4.23 (0.423) <sup>b</sup>	465 (12) <sup>c</sup>	WMCM (Weak) <sup>b</sup>
L-Valine	4.02 (0.402) <sup>b</sup>	NA <sup>d</sup>	WMCM (Weak) <sup>b</sup>
L-Glutamine	3.81 (0.381) <sup>b</sup>	NA <sup>d</sup>	WMCM (Weak) <sup>b</sup>
6-Phospho- gluconic acid	3.77 (0.377) <sup>b</sup>	14.4 (0.2) <sup>b</sup>	WMCM (Weak) <sup>b</sup>
Pyruvic acid	3.66 (0.366) <sup>b</sup>	15.8 (0.9) <sup>c</sup>	WMCM (Weak) <sup>b</sup>
Dihydroxyacetone phosphate	3.06 (0.306) <sup>b</sup>	20 (1) <sup>b</sup>	WMCM (Weak) <sup>e</sup>

<sup>a</sup>Uncertainty propagated from uncertainties in reagent masses and volumes used during sample preparation. Extra significant digits included to avoid systematic rounding errors in the statistical model.

<sup>b</sup>Determined at 37 °C with Isothermal titration calorimetry as measured in SI figure 1 and SI table 2. Error is the propagated standard error in the fit parameters.

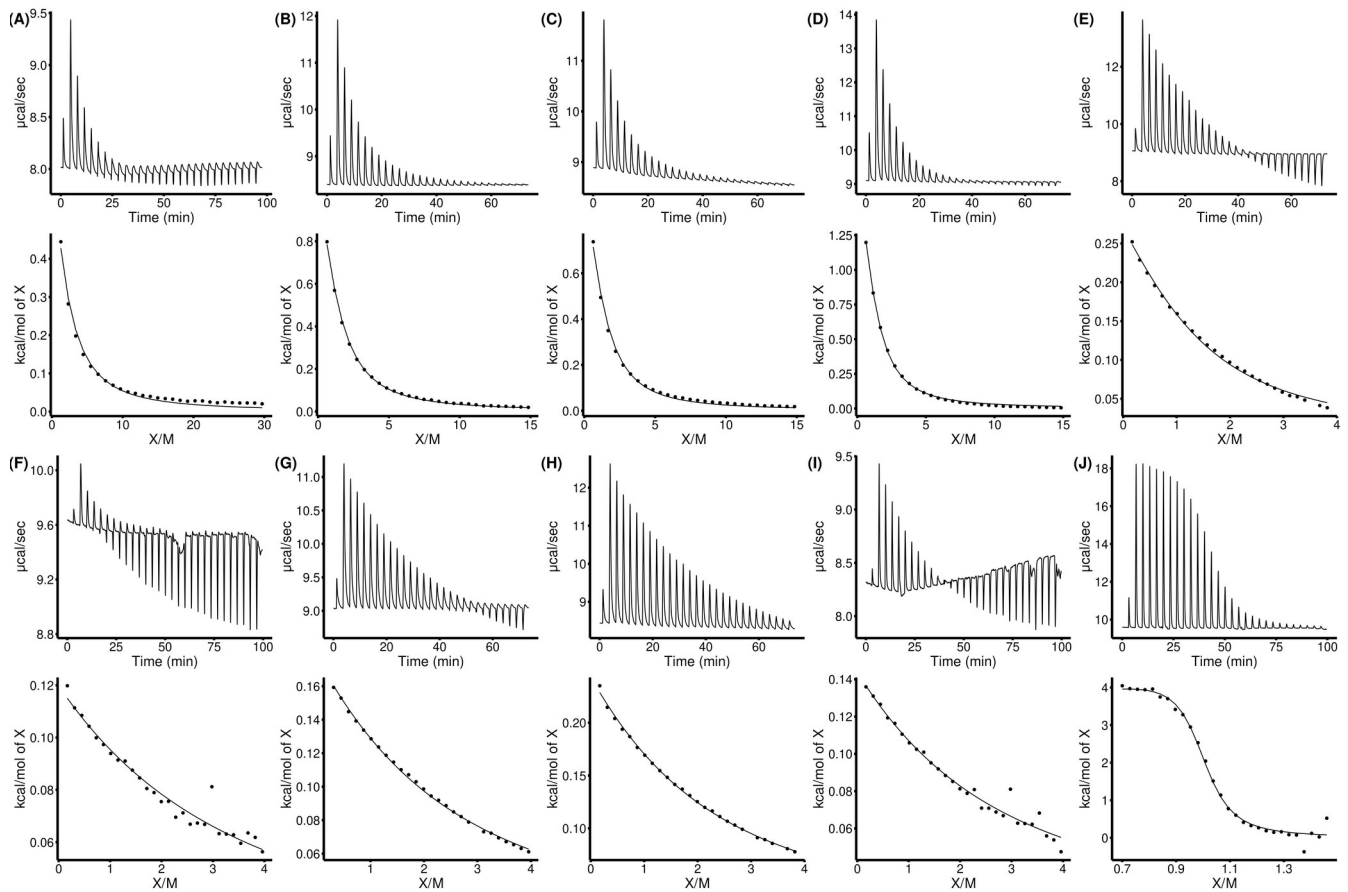
<sup>c</sup>Determined at 37 °C with HQS emission as measured in the SI figure 2 and SI table 3. Error is the propagated standard error in the fit parameters.

<sup>d</sup>No binding observed as per SI Figure 2.

<sup>e</sup>Metabolites with  $K_D$ s for Mg<sup>2+</sup> less than 2 mM are considered strong Mg<sup>2+</sup> chelators, while those greater than 2 mM are considered weak.

~27 mM

**SI Table 1.** Recipe for the Eco80 artificial cytoplasm (Add in later in word when I am formatting the tables)

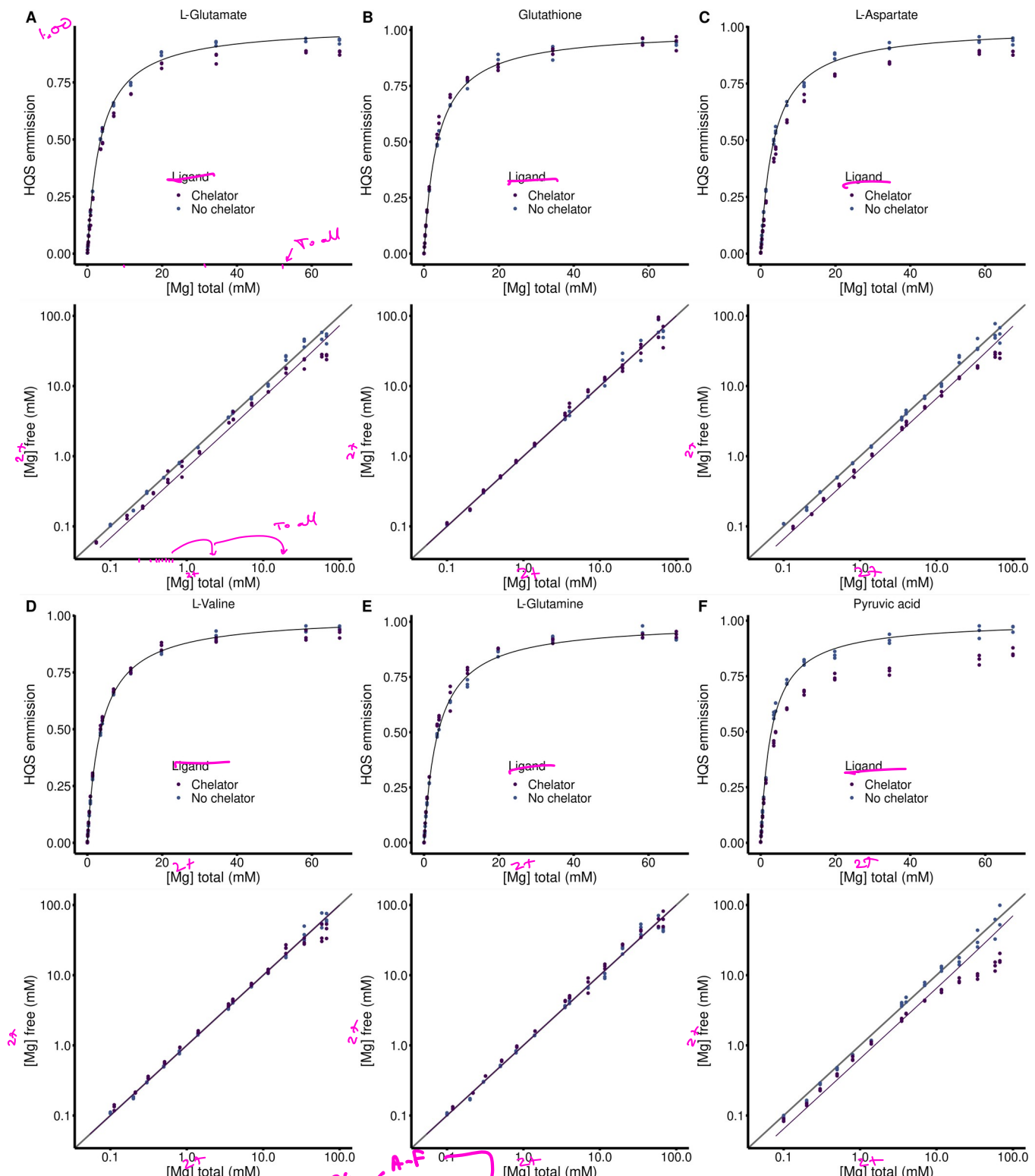


**SI Figure 1** Isothermal titration calorimetry (ITC) analysis of  $Mg^{2+}$  binding to metabolites in 240 mM NaCl 140 mM KCl 10 mM HEPES pH 7.0 at 37 °C.  $MgCl_2$  was titrated into metabolites and the power was monitored over time (Top panel). Heat of the injection was calculated by integrating the raw power curve, and the background heat of  $MgCl_2$  dilution, collected on buffer containing no metabolite, was subtracted to produce the isotherms in the bottom panels. Lines in bottom pannels represent fits to the Weismann isotherm equation to determine apparent association constants. **(A)** Adenosine triphosphate (ATP). **(B)** Uridine triphosphate (UTP). **(C)** Guanosine triphosphate (GTP). **(D)** deoxythymidine triphosphate (dTTP). **(E)** Fructose 1,6-bisphosphate. **(F)** Uridine diphosphate-N-acetylglucosamine. **(G)** Glucose 6-phosphate. **(H)** 6-phosphogluconic acid. **(I)** phosphoenol pyruvate. **(J)** Ethylene diamine-tetracetic acid (EDTA). Thermodynamic values are found in SI table 2.

**SI Table 2** Apparent binding constants determined with Isothermal titration calorimetry (ITC).

Metabolite	Syringe (mM)	Cell (mM)	$\Delta H$ (kcal/mol)	$K'$ ( $M^{-1}$ )	$K_D'$ ( $mM^{-1}$ )
ATP	15 mM MgCl <sub>2</sub> <sup>a</sup>	0.1 mM ATP <sup>a</sup>	1.83 (0.04)	3600 (200)	0.28 (0.01)
UTP	15 mM MgCl <sub>2</sub> <sup>a</sup>	0.2 mM UTP <sup>a</sup>	1.70 (0.01)	4200 (70)	0.248 (0.004)
GTP	15 mM MgCl <sub>2</sub> <sup>a</sup>	0.2 mM GTP <sup>a</sup>	1.43 (0.02)	5000 (200)	0.201 (0.007)
dTTP	15 mM MgCl <sub>2</sub> <sup>a</sup>	0.2 mM dTTP <sup>a</sup>	2.19 (0.02)	6300 (300)	0.160 (0.003)
Fructose 1,6-BP	100 mM MgCl <sub>2</sub> <sup>a</sup>	5.0 mM Fructose 1,6-BP <sup>a</sup>	0.414 (0.004)	169 (4)	5.9 (0.1)
UDP-GlcNAC	100 mM MgCl <sub>2</sub> <sup>a</sup>	5.0 mM UDP-GlcNAC	0.57 (0.02)	34 (2)	29 (2)
Glucose 6-P	100 mM MgCl <sub>2</sub> <sup>a</sup>	5.0 mM Glucose 6-P <sup>a</sup>	0.555 (0.003)	57.9 (0.7)	17.3 (0.2)
6-P-gluconic acid	100 mM MgCl <sub>2</sub> <sup>a</sup>	5.0 mM 6-P-gluconic acid <sup>a</sup>	0.662 (0.005)	70 (1)	14.4 (0.2)
Dihydroxyacetone phosphate	100 mM MgCl <sub>2</sub> <sup>a</sup>	5.0 mM dihydroxyacetone phosphate <sup>a</sup>	0.50 (0.01)	51 (3)	20 (1)
EDTA	6 mM MgCl <sub>2</sub> <sup>a</sup>	1.5 mM EDTA 1.0 mM MgCl <sub>2</sub> <sup>a,b</sup>	2.85 (0.04)	220,000 (30,000)	0.0045 (0.0006)

<sup>a</sup>240 mM NaCl 140 mM KCl 10 mM HEPES pH 7.0 at 37 °C<sup>b</sup>Mg<sup>2+</sup> and EDTA were incorporated into the cell in order to sequester trace tight binding metal ions and thereby negate their contribution to ITC signal.



**SI Figure 2** HQS analysis of  $Mg^{2+}$  binding to metabolites in 240 mM NaCl 140 mM KCl 20 mM MOPS 0.01 mM EDTA 0.001% SDS pH 7.0. (Top panels) Dependence of HQS emission on the total concentration of  $MgCl_2$  in the presence and absence of a metabolite chelators. Black lines represent a fit to SI equation 1 to determine the  $F_{\text{max}}$ ,  $F_{\text{min}}$ , and  $K_{\text{HQS}}$ . (Bottom panels) Dependence of the free  $Mg^{2+}$  concentration on the total concentration of  $MgCl_2$  in the presence and absence of a metabolite chelators. Grey lines represent where the free  $Mg^{2+}$  concentration equals the total concentration of  $MgCl_2$ , Purple lines represent a fit to SI equation 4 to determine the association constant between HQS and a chelator. (**A**)

240 mM L-glutamate. (B) 194 Glutathione. (C) 240 mM L-aspartate. (D) 240 mM L-valine. (E) 240 mM L-glutamine. (F) 5 mM pyruvic acid.

**SI Table 3** Apparent binding constants determined with HQS emission.  $F_{\max}$ ,  $F_{\min}$ , and  $K_{HQS}$  are determined by fitting HQS emission in the absence of chelators and used to calculate the free  $Mg^{2+}$  concentration in each sample. Metabolite binding constants,  $K'$  and  $K_D'$ , are determined by fitting the relationship between the free  $Mg^{2+}$  concentration and the total  $MgCl_2$  concentration using SI Equation 4.

Metabolite	$F_{\max}$	$F_{\min}$	$K_{HQS}$ ( $mM^{-1}$ )	$K'$ ( $mM^{-1}$ )	$K_D'$ ( $mM^{-1}$ )
L-Glutamic acid	187,000 (1000)	0 (810)	0.281 (0.008)	0.0019 (0.0002)	520 (50)
Glutathione	182,000 (1000)	592 (750)	0.279 (0.007)	NA <sup>c</sup>	NA <sup>c</sup>
L-Aspartic acid	196,000 (1000)	0 (820)	0.283 (0.007)	0.0021 (0.0001)	465 (12)
L-Valine	188,200 (800)	495 (580)	0.274 (0.005)	NA <sup>c</sup>	NA <sup>c</sup>
L-Glutamine	190,000 (1400)	516 (110)	0.27 (0.01)	NA <sup>c</sup>	NA <sup>c</sup>
Pyruvic acid	188,000 (1500)	0 (1300)	0.35 (0.01)	0.063 (0.003)	15.8 (0.9)

<sup>c</sup>No binding observed as per SI Figure 2

**SI Table 3.** HQS fits in the absence of chelators, used to determine free  $Mg^{2+}$  concentrations.  $F_{\max}$ ,  $F_{\min}$ , and  $K_{HQS}$  are determined by fitting HQS emission in the absence of chelators and used to calculate the free  $Mg^{2+}$  concentration in each sample.

Metabolite	$F_{\max}$	$F_{\min}$	$K_{HQS}$ ( $mM^{-1}$ )
Eco80	185,100 (800)	124 (1000)	0.239 (0.005)
NTPCM	187,000 (1500)	436 (1000)	0.26 (0.01)
WMCM	179,000 (1600)	0 (1400)	0.32 (0.01)

**Table 2.** Total  $Mg^{2+}$  concentrations used to obtain 2 mM free  $Mg^{2+}$  in artificial cytoplasm.

Condition	Total $[Mg^{2+}]$ ( $mM$ )	Chelated $[Mg^{2+}]$ ( $mM$ )	Free $[Mg^{2+}]$ ( $mM$ )
Eco80	31.6	29.6	2.0
NTPCM	25.0	23	2.0
WMCM	6.4	4.5	2.0

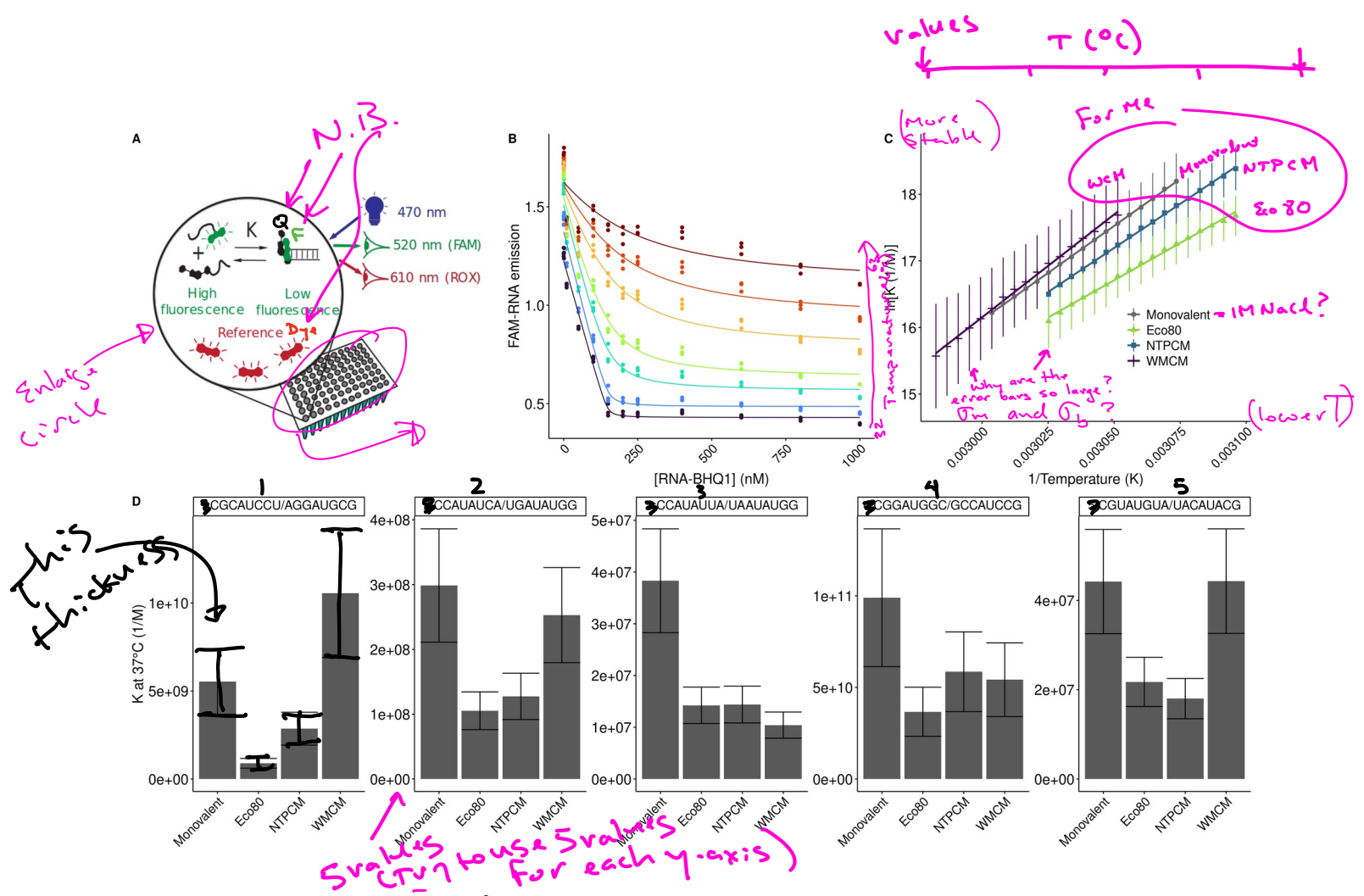
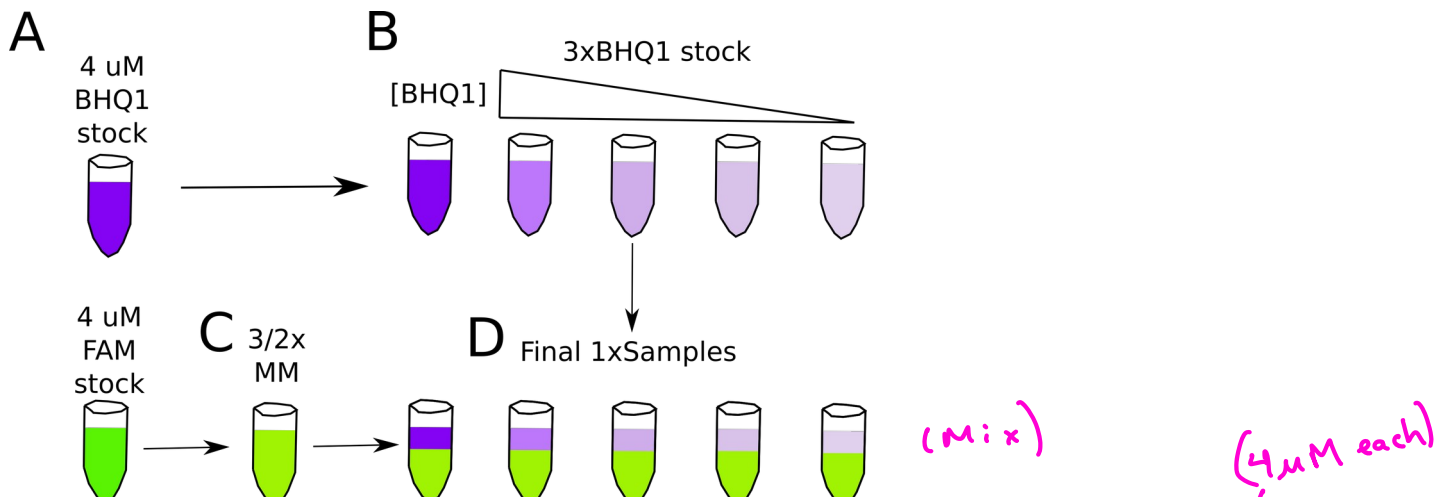
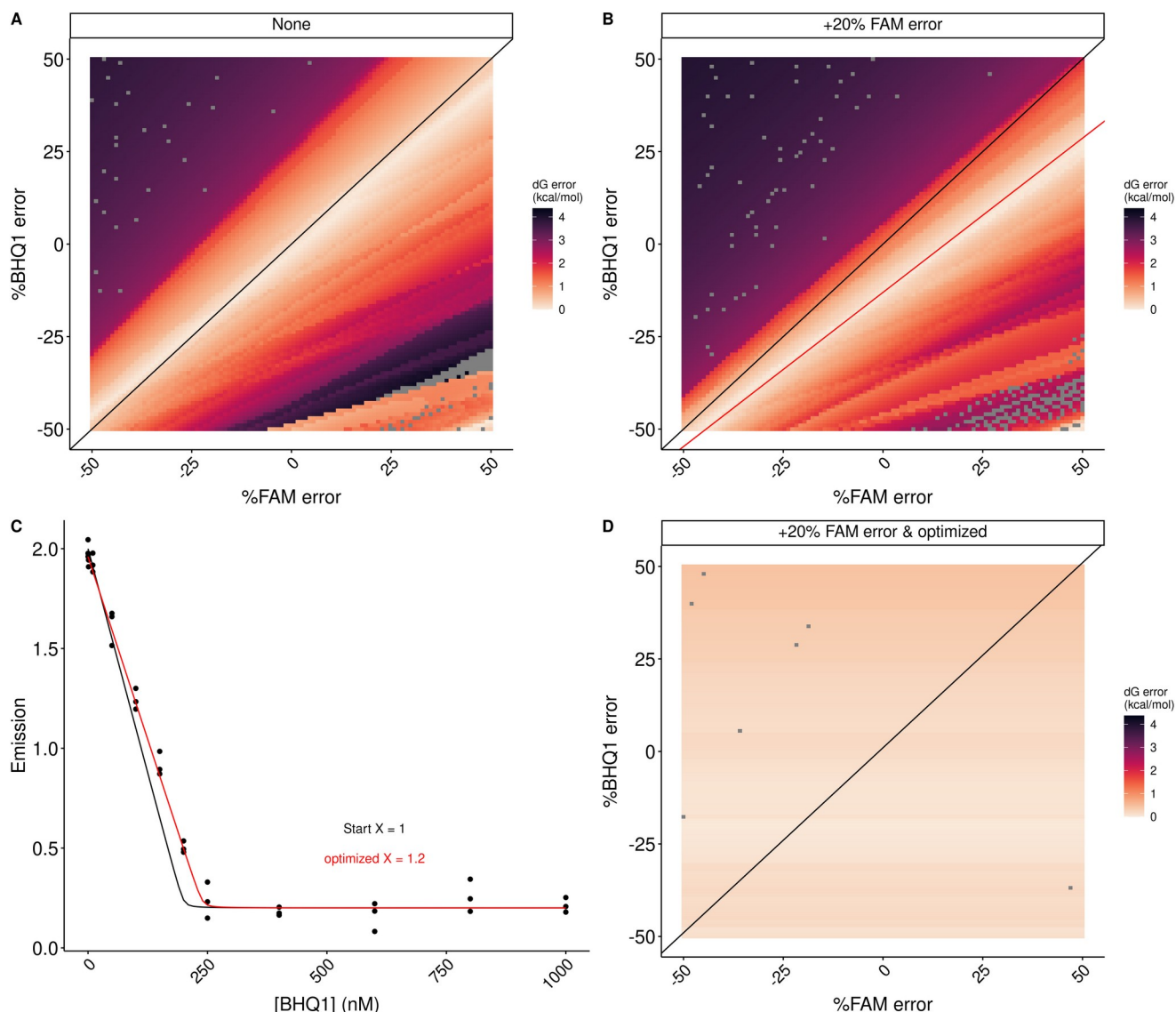


**Figure 2** *E. coli* metabolite and  $Mg^{2+}$  mixtures destabilize RNA secondary structure. Helix folding energies in Eco80, NTPCM, and WMCM were determined using fluorescence binding isotherms that are fit with the MeltR program. **(A)** Layout of a fluorescence binding isotherms assay to determine helix folding energies in Eco80, NTPCM, and WMCM, in a Real-Time PCR machine. **(B)** Raw fluorescence binding isotherms fit to determine equilibrium constants with MeltR. Data points represent raw data. Curves represent curve fits. Colors represent different temperatures (purple: 32.3, blue: 41.8, teal: 51.3, green: 54.6, yellow: 58.4, orange: 60.7, red: 63.1 °C). **(C)** Van't Hoff relationship between equilibrium constant and temperature for helix 1:CGCAUCCU/AGGAUGCG folding in background monovalent metal ions (240 mM NaCl 140 mM KCl), Eco80, NTPCM, and WMCM. All conditions contain 2 mM free  $Mg^{2+}$ . Points and error bars represent association constants and standard errors propagated from the fit (using MeltR). Lines represent the fits to the Van't Hoff equation that MeltR uses to calculate folding energies. The y-axis uses the association constant ( $K$ ) instead of the dissociation constant ( $K_D$ ) because  $K_D$  are proportional to stability.  $K = 1/K_D$ . A shift in the Van't Hoff relationship, down and to the right of the plot area, indicates that Eco80 destabilizes the helix. **(D)** The association constant ( $K$ ) at 37 °C in Eco80, NTPCM, and WMCM compared to the  $K$  at 37 °C in background monovalent metal ions (240 mM NaCl 140 mM KCl), for five RNA helices. All conditions contain 2 mM free  $Mg^{2+}$ . Errors were propagated assuming 1% uncertainty in the Gibb's free energy at 37 °C.

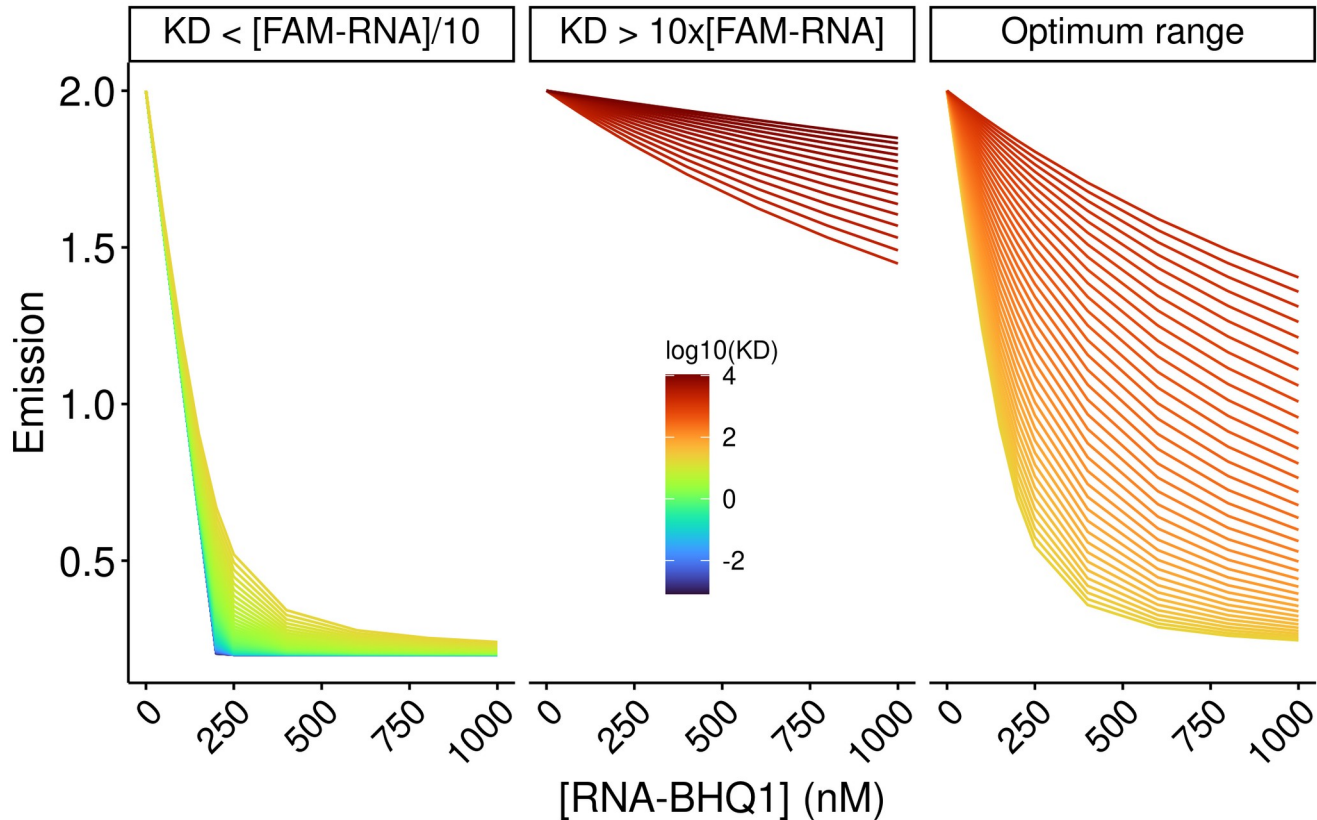
Less in  $\Delta G$ . Can /  
should we show this  
somehow?



**SI figure 3** Errors in the determination of concentrations of RNA stocks are systematically propagated during sample prep for fluorescence isotherm experiments. **(A)** FAM-RNA and RNA-BHQ1 stock concentrations are determined at a low  $\mu$ M concentrations with UV-absorbance. In this work, FAM and BHQ1 stocks were prepared at the same concentration, 4  $\mu$ M. **(B)** RNA-BHQ1 stocks are diluted to a 3x concentration from one stock. **(C)** FAM-RNA stocks were diluted to a 3/2x concentration into artificial cytoplasm to make a master mix (MM). **(D)** One volume of 3xRNA-BHQ1 stock is mixed with two volumes of 3/2xMM to prepare the final solution.



**SI figure 4** The concentration optimization algorithm improves the accuracy of helix folding energies calculated with MeltR using data with inaccurate RNA concentration estimates. **(A)** Error in the Gibbs free energy (dG) calculated with MeltR on modeled data assuming perfectly accurate RNA concentration estimates is reduced when the %FAM-RNA concentration error and %RNA-BHQ1 concentration error compensates according to the black line, %FAM-RNA error = %RNA-BHQ1. Data were modeled assuming a folding enthalpy ( $\Delta H$ ), entropy ( $\Delta S$ ), and Gibb's free energy at 37 °C ( $\Delta G$ ) of -56.2 kcal/mol, -136.4 cal/mol/K, and -13.9 kcal/mol respectively, and 5% random fluorescence error. Concentration errors were seeded into the modeled data and the data was fit with MeltR. **(B)** Error in the Gibbs free energy (dG) calculated with MeltR on modeled data, assuming a +20% FAM-RNA concentration estimate, is reduced when the %FAM-RNA concentration error and %RNA-BHQ1 concentration error compensate according to the red line, %RNA-BHQ1 = X \* %FAM-RNA error + (100 - 100 \* X) / X, where X is the factor the MeltR concentration optimization algorithm multiplies the FAM-RNA concentration estimate by. Data were modeled assuming a folding  $\Delta H$ ,  $\Delta S$ , and  $\Delta G$  of -56.2 kcal/mol, -136.4 cal/mol/K, and -13.9 kcal/mol respectively, 5% random fluorescence error, and a +20% increase in the FAM-RNA concentration. Additional concentration errors were seeded into the modeled data and the data was fit with MeltR. **(C)** MeltR identifies the FAM-RNA concentration correction factor (X) using a low temperature fluorescence isotherm as a Job plot. Black data points represent modeled fluorescence data from B at 20 °C. The black line represents the shape of the curve with a X of 1. The red line represents the shape of the curve with an optimized X of 1.2. **(D)** Error in the Gibbs free energy (dG) calculated with MeltR using the concentration optimization algorithm and the data from B. On average, MeltR estimates the correct  $\Delta G$  within 0.2 kcal/mol, using the concentration optimization algorithm.



**SI figure 5**  $K_D$ s calculated using MeltR are most accurate between the FAM-RNA concentration/10 and 10 times the FAM-RNA concentration. At  $K_D$ s that are more than 10 fold lower than the FAM-RNA concentration, the shape of the curve is independent of the  $K_D$ . At  $K_D$ s more than 10 fold higher than the FAM-RNA concentration, there is very little dependence of FAM-RNA emission on RNA-BHQ1 concentration. However, the curve shape is highly dependent on  $K_D$  within the optimum range, so MeltR allows the user to specify an optimum  $K_D$  range to calculate helix folding energies.

**SI table 4. Stability of RNA helices in *E. coli* metabolite mixtures. Helix energy was calculated by fitting raw fluorescence data with MeltR. Standard errors are estimated from fits. Extra significant digits are included to avoid propagating rounding errors.**

Sequence <sup>a</sup>	Condition <sup>b</sup>	X <sup>c</sup>	Method 1 VH plot ΔH kcal/mol	Method 1 VH plot ΔS cal/mol/K	Method 1 VH plot ΔG kcal/mol	Method 2 Global fit ΔH kcal/mol	Method 2 Global fit ΔS cal/mol/K	Method 2 Global fit ΔG kcal/mol	%Diff. <sup>d</sup> ΔG	%Diff. <sup>d</sup> ΔS	%Diff. <sup>d</sup> ΔG
1:CGCAUCCU/ AGGAUGCG	2 mM free	1.3	-55.9 (0.2)	-136.0 (0.7)	-13.82 (0.01)	-56.0 (8.9)	-135.9 (27.0)	-13.8 (0.5)	0.2%	0.1%	0.1
	NTPCM	2	-52.2 (0.4)	-125 (1)	-13.41 (0.02)	-52.4 (7.6)	-125.6 (23.2)	-13.4 (0.4)	0.4%	0.5%	0.1%
	WMCM	1.0	-61.4 (0.8)	-152 (2)	-14.22 (0.05)	-61.1 (14.0)	-151.2 (42.5)	-14.2 (0.9)	0.5%	0.5%	0.1%
	Ecoli80	1.5	-44.5 (0.7)	-102 (2)	-12.70 (0.04)	-44.4 (7.6)	-102.1 (23.3)	-12.7 (0.4)	0.2%	0.1%	0.0%
2: CCAUAUCA/ UGAUUAUGG	2 mM free	0.9	-53.4 (1.0)	-133 (3)	-12.02 (0.04)	-52.3 (14.9)	-129.9 (43.2)	-12.0 (0.5)	2.1%	2.4%	0.2%
	NTPCM	1.3	-42.9 (0.5)	-101 (1)	-11.50 (0.02)	-42.4 (20.4)	-99.6 (63)	-11.5 (0.8)	1.2%	1.4%	0.0%
	WMCM	1.0	-53 (2)	-132 (7)	-11.9 (0.1)	-51.6 (5.3)	-128.0 (1.6)	-11.9 (0.2)	2.7%	3.1%	0.0%
	Ecoli80	0.9	-57 (2)	-146 (5)	-11.38 (0.05)	-54.0 (13.1)	-137.7 (-41.1)	-11.3 (0.4)	5.4%	5.9%	0.7%
3: CCAUAAUA/ UAAAUAUGG	2 mM free	0.9	-53.5 (0.4)	-137 (1)	-10.76 (0.01)	-53.2 (8.4)	-136.7 (27.1)	-10.8 (0.1)	0.6%	0.2%	0.4%
	NTPCM	1.0	-45.0 (0.2)	-112.5 (0.5)	-10.158 (0.002)	-45.0 (8.0)	-112.2 (25.6)	-10.2 (0.1)	0.0%	0.3%	0.4%
	WMCM	0.8	-43 (2)	-107 (5)	-9.94 (0.02)	-40.5 (9.3)	-98.4 (29.6)	-9.9 (0.1)	6.0%	8.4%	0.4%
	Ecoli80	1.2	-41.3 (0.2)	-100.4 (0.7)	-10.15 (0.01)	-41.2 (9.2)	-100.3 (29.4)	-10.2 (0.2)	0.2%	0.1%	0.5%
4: CGGAUGGC/ GCCAUCCG	2 mM free	1.1	-71.1 (0.8)	-179 (2)	-15.6 (0.06)	-71.3 (15.6)	-179.6 (46.6)	-15.6 (1.1)	0.3%	0.3%	0%
	NTPCM	1.2	-70.4 (0.6)	-177 (2)	-15.28 (0.05)	-70.5 (15.1)	-178.0 (45.2)	-15.3 (1.0)	0.1%	0.6%	0.1%
	WMCM	1.1	-65.5 (2)	-162 (7)	-15.2 (0.2)	-65.3 (12.2)	-161.6 (36.4)	-15.2 (0.9)	0.3%	0.2%	0%
	Ecoli80	1.0	-69.7 (0.8)	-176 (3)	-15.0 (0.1)	-69.6 (11.4)	-176.3 (34.2)	-15.0 (0.8)	0.1%	0.2%	0.2%
5: CGUAUGUA/ UACAUACG	2 mM free	0.8	-63.2 (0.9)	-169 (3)	-10.85 (0.02)	-62.3 (7.3)	-165.9 (23.0)	-10.8 (0.1)	1.4%	1.9%	0.5%
	NTPCM	0.9	-59 (1)	-157 (4)	-10.30 (0.01)	-58.5 (7.6)	-155.5 (24.3)	-10.3 (0.1)	0.9%	1.0%	0.0%
	WMCM	1.0	-67 (1)	-180 (3)	-10.85 (0.02)	-66.1 (10.5)	-178.1 (33.2)	-10.8 (0.2)	1.4%	1.1%	0.1%
	Ecoli80	1.0	-61 (1)	-164 (3)	-10.41 (0.01)	-60.9 (4.09)	-162.9 (13.1)	-10.4 (0.06)	0.2%	0.7%	0.2%
Average %error			1.7%	2.0%	0.3%	21.7%	26.5%	3.4%	1.2%	1.4%	0.2%

<sup>a</sup>The first sequence was 5'-FAM labeled and the second sequence was 3'-BHQ1 labeled.

<sup>b</sup>All solutions contain 2 mM Free Mg, 240 Na<sup>+</sup> 140 mM K<sup>+</sup>.

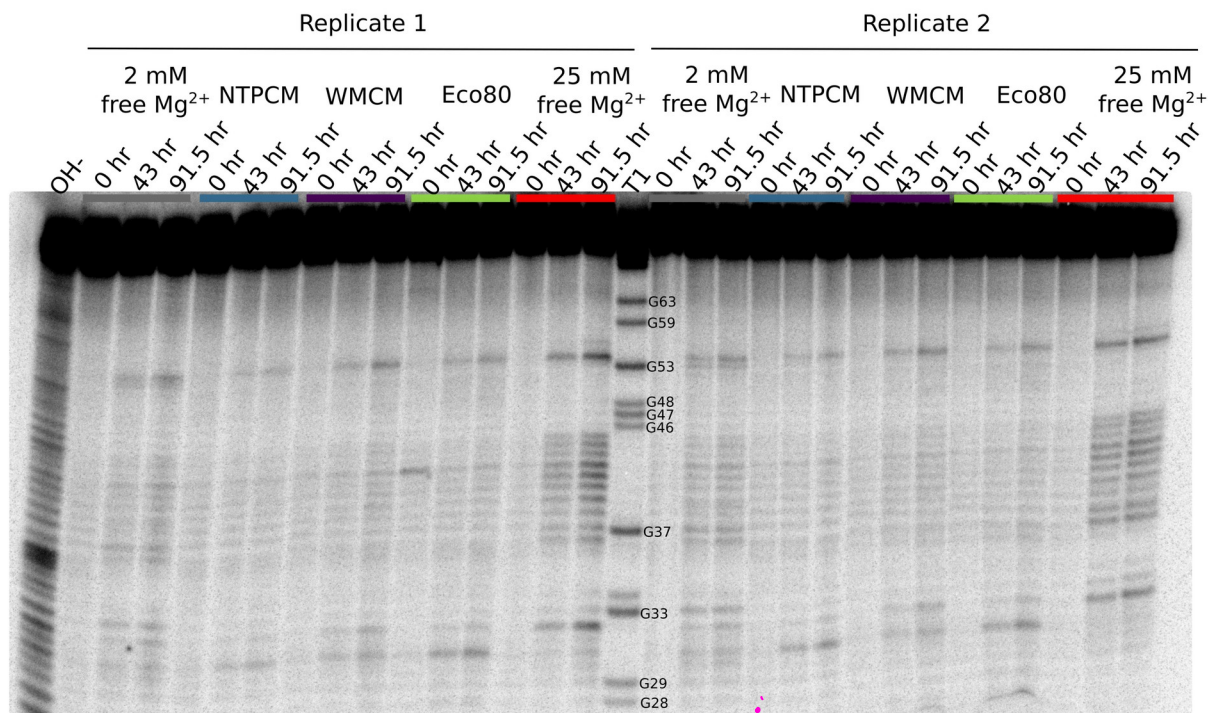
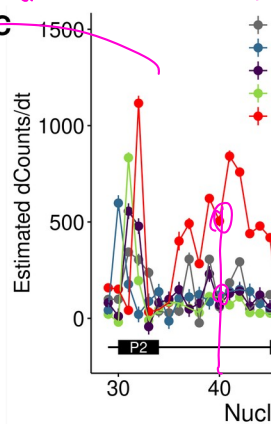
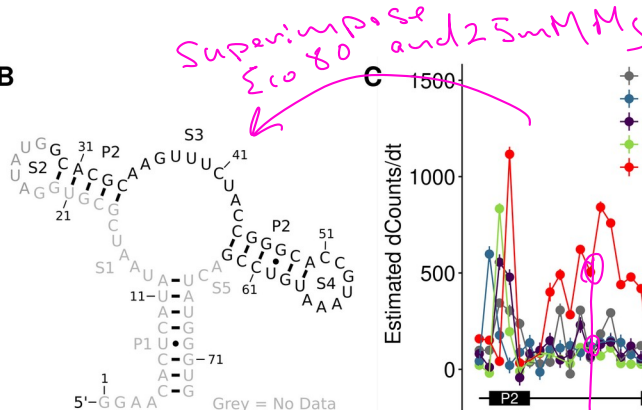
<sup>c</sup>Concentration optimization factor used to correct FAM-RNA concentrations by MeltR.

<sup>d</sup>Percent difference between Method 1 and Method 2.

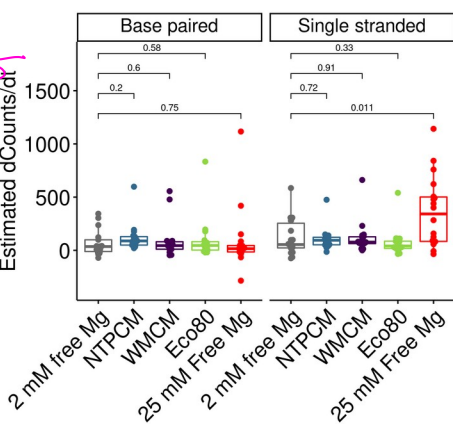
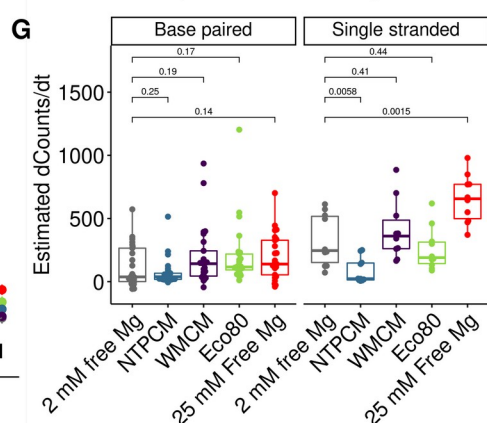
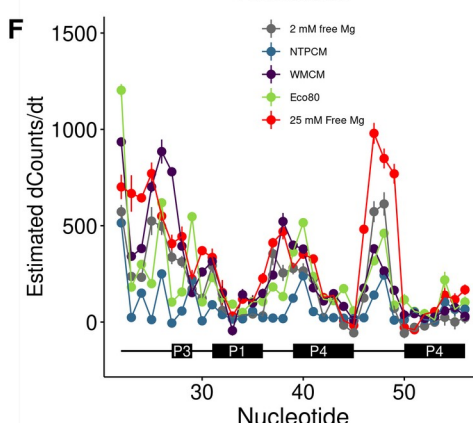
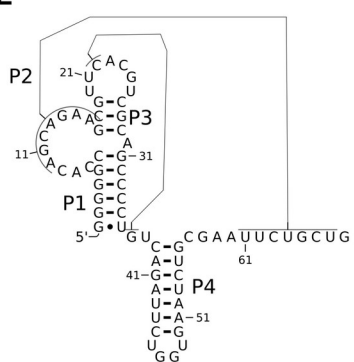
**Table 3. Stability of RNA helices in *E. coli* metabolite mixtures.**

Sequence <sup>a</sup>	AU content	Condition <sup>b</sup>	ΔG (kcal/mol) <sup>c</sup>	ΔΔG (kcal/mol) <sup>c</sup>
1: CGCAUCCU/ AGGAUGCG	0.38	2 mM free	-13.82 (0.21)	
		NTPCM	-13.41 (0.20)	0.41 (0.29)
		WMCM	-14.22 (0.21)	-0.40 (0.30)
		Ecoli80	-12.70 (0.19)	1.12 (0.28)
2: CCAUAUCA/ UGAUUAUGG	0.63	2 mM free	-12.02 (0.18)	
		NTPCM	-11.50 (0.17)	0.52 (0.25)
		WMCM	-11.90 (0.18)	0.12 (0.25)
		Ecoli80	-11.38 (0.17)	0.64 (0.25)
3: CCAUAAUA/ UAAUAUGG	0.75	2 mM free	-10.76 (0.16)	
		NTPCM	-10.16 (0.15)	0.60 (0.22)
		WMCM	-9.94 (0.15)	0.82 (0.22)
		Ecoli80	-10.15 (0.15)	0.61 (0.22)
4: CGGAUGGC/ GCCAUCCG	0.25	2 mM free	-15.60 (0.23)	
		NTPCM	-15.28 (0.23)	0.32 (0.33)
		WMCM	-15.20 (0.23)	0.40 (0.33)
		Ecoli80	-15.00 (0.23)	0.60 (0.32)
5: CGUAUGUA/ UACAUACG	0.63	2 mM free	-10.85 (0.16)	
		NTPCM	-10.30 (0.15)	0.55 (0.22)
		WMCM	-10.85 (0.16)	0.00 (0.23)
		Ecoli80	-10.41 (0.16)	0.44 (0.23)

<sup>a</sup>The first sequence was 5'-FAM labeled and the second sequence was 3'-BHQ1 labeled.<sup>b</sup>All solutions contain 2 mM Free3 Mg, 240 Na<sup>+</sup> 140 mM K<sup>+</sup>.<sup>c</sup>Extra significant digits were included to avoid propagating rounding errors.

**A****B**

*25 mM Mgs*  
Eco 80  
?

**E**

**Figure 3** *E. coli* metabolite and Mg<sup>2+</sup> mixtures stabilize the chemical structure of RNA. **(A)** Raw degradation assay gel image for the Guanine riboswitch aptamer incubated in artificial cytoplasms at 37 °C and pH 7. The

OH- lane contains a hydrolysis ladder which cleaves after every nucleotide and T1 contains the RNA treated with T1 ribonuclease which cleaves after every G. Enough Mg<sup>2+</sup> was added to each artificial cytoplasm to have 2 mM Mg<sup>2+</sup> as determined in Figure 1. **(B)** Secondary structure of the guanine riboswitch aptamer. **(C)** Estimated increase in counts as a function of time at each residue in different solution conditions as a function of location in the RNA. **(D)** Estimated increase in counts as a function of time in different conditions grouped by paired and unpaired bases. Significance was determined using a student's t-test. **(E)** Secondary structure of the cleaved human CPEB3 HDV ribozyme. **(C)** Estimated increase in counts as a function of time at each residue in different solution conditions as a function of location in the RNA. **(D)** Estimated increase in counts as a function of time in different conditions grouped by paired and unpaired bases. Significance was determined using a student's t-test.

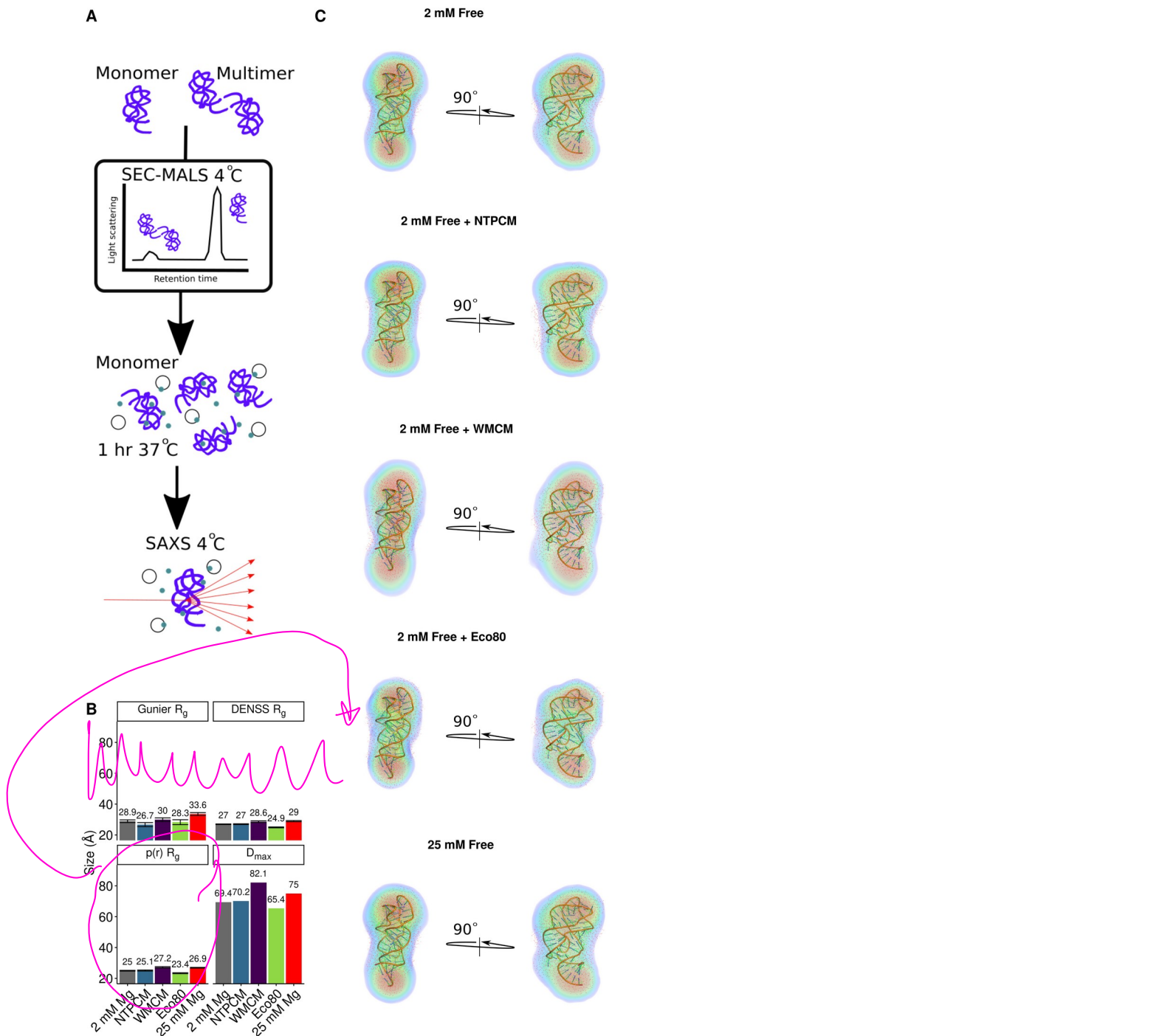


**Figure 4** *E. coli* metabolite and  $Mg^{2+}$  mixtures increase functional RNA compactness.